

# [Chapter 1: Introduction]

---

## 1 Introduction

Over the last few decades, the mixed oxide materials have emerged as one of the most engaging research areas for the condensed matter physicists and material scientists. To understand the properties of materials existing from earlier times to the newly developed device technology both theoretical and experimental methods have been intensively used. Among all oxide materials, the manganites form an important class [1, 2]. The manganites which normally possess perovskite type structure have unique and fascinating properties that have broad impact on both the basic and applied research [3]. As most of the technology pursued using this material requires proper film growth, extensive efforts are made on material synthesis, structural and physical characterization and device fabrication. Furthermore, the recent and modern works have been driven by a desire to comprehend and utilize the large negative magnetoresistance effect which occurs near and below the Curie temperature ( $T_C$ ). These compounds are the real example of the interplay between experiment, theory and application which are the heart of Condensed Matter and Materials Physics.

### 1.1 Introduction to Manganite Materials and Magnetoresistance

The mixed-valence manganese oxide perovskites also known as manganites are still considered as the modern materials and receive tremendous attention not only from the field of basic science but also from the current cutting-edge technology [4]. Out of many interesting properties of manganites, the most fascinating property is the Colossal Magnetoresistance (CMR) which is currently being explored by a sizable fraction of the condensed matter community and its popularity is reaching almost the same level that of the one-time popular high temperature superconducting cuprates. The CMR is an intrinsic property of manganese based perovskite oxides that displays changes in resistance with significant orders of magnitude under

## [Chapter 1: Introduction]

the influence of an external magnetic field. The perovskite manganites possessing CMR property are strongly correlated electron systems with strong interplays among the charge, spin, orbital, and lattice degrees of freedom that leads to complex structural, electronic, phonon and magnetic properties [5-8]. The physics involved in manganites include double exchange (DE) mechanism [9, 10], Jahn-Teller distortion [11, 12], size variance and fascinating metallic behavior making them one of the prominent topics in the field of condensed matter physics. Due to the advent of excellent and upto date technology, various prototypes are manufactured using various synthesis processes. The manganites also have potential applications in the solid electrolytes, catalysts, sensors, solid state memories and magnetic microwave devices [13-15]. Some of the other important applications of manganites are magnetic refrigeration, advanced hard disk read heads, recording devices, bottom electrode in the fabrication of ferroelectric memories, etc. [16]. The CMR effect further influences the metal-to-insulator (MIT) transition, the nature of electronic transport, charge-ordering, magnetism etc. [17-21]. The MIT coincides with the ferromagnetic to paramagnetic transition [22]. Fig. 1.1 (a) shows the temperature and magnetic field variations of resistivity for a  $\text{La}_{0.75}\text{Ca}_{0.25}\text{MnO}_3$  manganite [23]. The figure depicts a dramatic drop in resistivity with the increase in magnetic field with a shift in peak to higher temperatures. Fig.1.1 (b) displays magnetoresistance percentage (MR%) as a function of applied magnetic field.

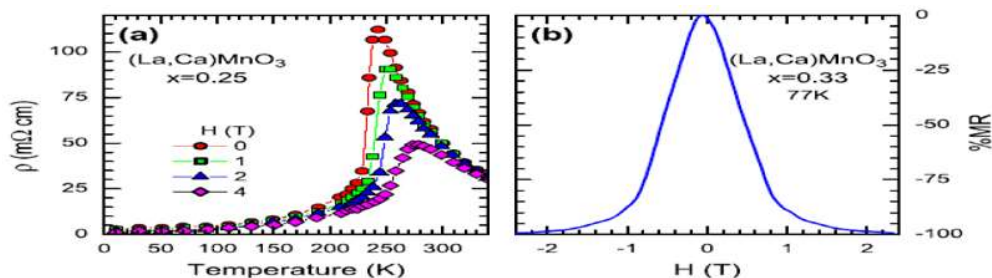


**Fig. 1.1:** Magnetic-field dependent resistivity in  $(\text{La,Ca})\text{MnO}_3$  (a) Resistivity versus temperature for  $x = 0.25$  at different applied magnetic field (b) Magnetoresistance as a function of applied magnetic field for  $x = 0.33$  [23].

## [Chapter 1: Introduction]

---

Manganites exhibit a variety of phases such as paramagnetic state, ferromagnetic metal or insulator, anti-ferromagnetism, canted anti-ferromagnetism and charge ordering. Many properties of CMR materials can be tuned by varying the external parameters such as temperature (T), magnetic field (H) or by the chemical pressure i.e. by doping. The manganite systems belong to the crystallographic class of the perovskites with stoichiometry  $ABO_3$  (see Fig. 1.2). The  $LaMnO_3$  crystallizes in this type of structure in which La and Mn atoms occupy A and B-sites respectively (see Fig. 2). The  $MnO_6$  octahedron is shown at the corner of the unit cell. However, for a stable  $ABO_3$  perovskite, existence of stable and polar, octahedral-site building blocks is prerequisite.

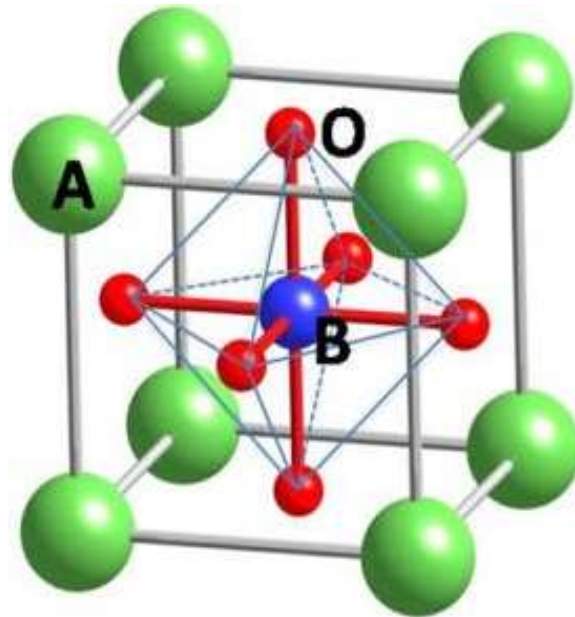


**Fig. 1.2:** An  $ABO_3$  type of perovskite structure.

In rare-earth manganites, distortions from the ideal cubic perovskite structure subsequently reduce the symmetry as going from cubic to orthorhombic, rhombohedral, tetragonal, or monoclinic phase [19]. In this structure, A (La) ion occupies the position at the center of the cubic cell while B (Mn) ions occupy octahedral positions at the boundaries enclosed

---

## [Chapter 1: Introduction]

---

by six oxygen ions positioned at the edge-center of the cell and the  $\text{MnO}_6$  octahedra [24]. The cations Mn and La have 3+ oxidation states. Rare-earth manganites have general chemical formula  $\text{R}_{1-x}\text{A}_x\text{MnO}_3$  (R is a trivalent rare-earth element La, Pr, Nd, etc. and A is an alkali earth element Ca, Sr, Ba, etc.). Since Mn exists in mixed valence state, these compounds are also known as “mixed-valent manganites”. When,  $0 < x < 0.5$ ,  $\text{Mn}^{4+}$  content is less than 50% and holes are the charge carriers, hence possess positive type conductivity. The p-type or hole doped manganites exhibit ferromagnetic metallic (FMM) behavior below a certain critical temperature and a certain minimum amount of  $\text{Mn}^{4+}$ . It has been reported that the largest transition is observed for  $x = 0.33$  [18-21].

### 1.2 Types of Magnetoresistance

There exist four types of magnetoresistance due to different physical origins.

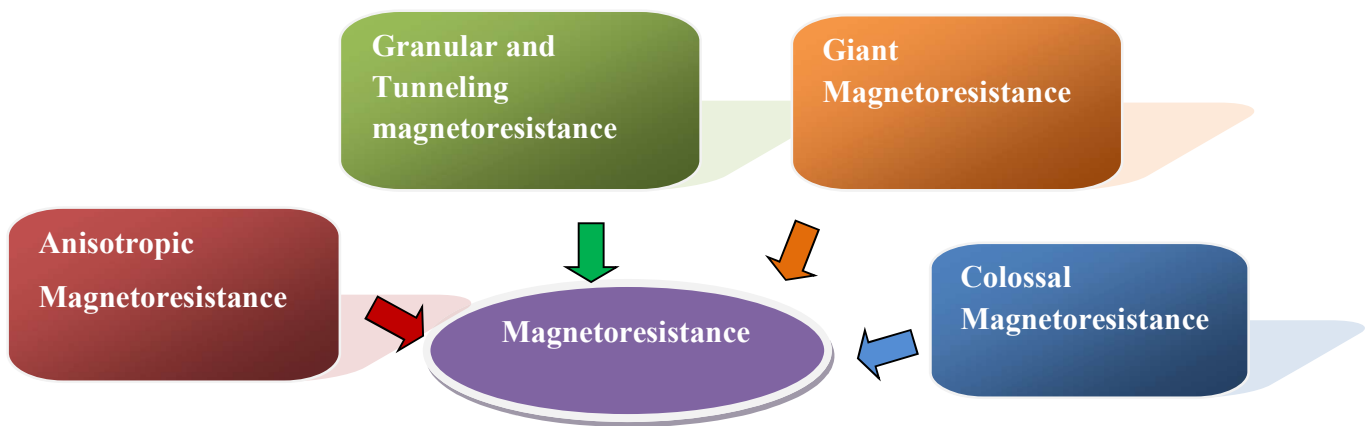


**Fig. 1.3:** Types of the Magnetoresistance.

#### A. Anisotropic Magnetoresistance (AMR)

This arises due to the electrical resistance dependence on the angle between the direction of electric current and magnetization [25, 26]. In certain ferromagnetic metallic systems, the resistivity increases or decreases when applied magnetic field is perpendicular or parallel to the

## [Chapter 1: Introduction]

---

direction of the electric current. The classical formula for the anisotropic magnetoresistance can be expressed as,

$$\frac{\Delta\rho}{\rho} = \rho_{||} - \rho_{\perp} / \rho_{\perp} \quad (1)$$

Where,  $\rho_{||}$  and  $\rho_{\perp}$  are resistances with the applied magnetic field in parallel and perpendicular direction to the sample respectively. This effect is normally low and lies in the range of 1 - 2% at room temperature [27].

### **B. Granular and Tunneling Magnetoresistance (TMR)**

The second important type of magnetoresistance is the granular and tunneling magnetoresistance (TMR) originally discovered by M. Jullière [28]. It mainly arises in the granular systems due to the spin dependent scattering of carriers either at the grain boundaries or at the insulating barrier [29, 30]. The granular and tunneling magnetoresistance (TMR) is defined as [31]

$$\text{TMR} = R_{\text{ap}} - R_{\text{p}} / R_{\text{p}} \quad (2)$$

Where  $R_{\text{ap}}$  and  $R_{\text{p}}$  are the electrical resistance in the anti-parallel state resistance in the parallel state respectively.

### **C. Giant Magnetoresistance (GMR)**

A quantum mechanical magnetoresistance also known as giant magnetoresistance is observed in multilayers composed of alternating ferromagnetic and non-magnetic conducting layers which was first observed on the application of magnetic field on the atomically engineered magnetic superlattices such as Fe/Cr, Co/Cu multilayers [32].

The effect is observed as a significant change in the electrical resistance depending on whether the magnetization of adjacent ferromagnetic layers are in a parallel or an anti-parallel alignment. The overall resistance is relatively low or high for parallel or anti-parallel alignment

---

## [Chapter 1: Introduction]

---

respectively. This kind of magnetoresistance in which the electrical resistance of a sample depends on the strength of an external magnetic field is characterized by the equation,

$$\delta_H = \frac{R(H)-R(0)}{R(0)} \quad (3)$$

Where  $R(H)$  is the Hall resistance of the sample in a magnetic field  $H$ , and  $R(0)$  corresponds to  $H = 0$  field [33]. Owing to large amount of MR, the name Giant magnetoresistance was coined to emphasize the strength of MR in these materials.

### **D. Colossal Magnetoresistance (CMR)**

The origin of CMR in perovskite material is quite different from the other forms of magnetoresistance discussed above. The first theoretical description to CMR was given in terms of double-exchange mechanism in mixed valence perovskite manganites. The MR as large as ~100% has been observed in manganites during recent years [23]. To emphasize the strength of extraordinarily large MR, scientists coined a new term called “Colossal Magnetoresistance (CMR)” [34, 35]. The CMR effect is an intrinsic property of crystal structure and has its origin subjected to the spin disorder of conduction electrons and can be suppressed by magnetic field resulting in large magnetoresistance [36, 37]. The discovery of CMR effect in manganites and its relation to various electronic and magnetic properties revived the research interest in similar compounds. The CMR can be defined as,

$$MR\% = \rho_0 - \rho_H / \rho_0 \times 100 \quad (4)$$

Where,  $\rho_H$  and  $\rho_0$  are the resistivity at a given temperature in the presence and in absence of the external magnetic field, respectively. The positive MR% is commonly referred to as the ordinary magnetoresistance (OMR). Though, the research in preferable magnetoresistive materials has been in focus since early nineties, the perovskite structured oxide materials of type  $R_{1-x}A_xMnO_3$  ( $R$  = trivalent rare-earth cation,  $A$  = divalent cation) appeared in the center of

---

## [Chapter 1: Introduction]

---

observation for research, after the work of Von Helmholtz et al. [36] and Charara et al. [37] using a method employed for structurally similar high-temperature superconductors.

### 1.3 Factors Affecting CMR Manganites

#### 1.3.1 Tolerance Factor (t) and Crystal Structure

The arrangement of atoms in the cubic perovskite manganites is shown in Fig. 1.2. The space group depends on the obtained crystal structure of the synthesized material. The structure of parent compound  $\text{LaMnO}_3$  is of cubic perovskite. The unit cell consists of one A ion at (0, 0, 0), Mn ion at (0.5, 0.5, 0.5) and three O ions at (0, 0.5, 0.5), (0.5, 0, 0.5) and (0.5, 0.5, 0) positions of crystal axis. The A ion has 3+ valency while the O ion has 2- valency. This gives rise to Mn with the 3+ valence state to maintain the charge neutrality. When an A' ion (A' = alkaline earth) in 2+ valence state is doped at A site, the charge neutrality condition leads to a mixed valent state of Mn. Further the structure can be considered as stacking of two planes, AO and  $\text{MnO}_2$  one after one. It is known that the face diagonal A-O-A for an ideal cubic structure is  $\sqrt{2}$  times the cube edge, O-B-O; i.e,  $2 r_A + r_O = \sqrt{2} (2r_{\text{Mn}} + 2r_O)$ , where,  $r_A$ ,  $r_O$  and  $r_{\text{Mn}}$  are the radius of A, O and Mn ions respectively. However, in the case of doped system, the atomic radius  $r_A$  gets modified.

The tolerance factor 't' is defined as [38],

$$t = \frac{d_{\text{A-O}}}{\sqrt{2}d_{\text{Mn-O}}} = \frac{r_A + r_O}{\sqrt{2}(r_{\text{Mn}} + r_O)} \quad (5)$$

Hence, now  $r_A$  is used as average radius of A and A' ions. The tolerance factor t which is affected by ionic radius of A and A' signifies the manganite structure. The cubic structure of perovskite is stable for the tolerance values lying between 0.89 and 1.02 (i.e.  $0.89 < t < 1.02$ ). However, a large deviation from the unity leads to different crystal structures such as

## [Chapter 1: Introduction]

---

monoclinic, orthorhombic, hexagonal etc. The value of  $r_A$  in  $\text{La}_{1-x}\text{Sr}_x\text{MnO}_3$  (LSMO) is less than the ideal value 1.48 Å for the cubic crystal structure. This results into the rotation or distortion of  $\text{MnO}_6$  octahedra. The change in structure arising from this gives an orthorhombic, rhombohedral or monoclinic type of crystal structure which in turn affects the electronic and other properties of the CMR materials.

### 1.3.2 Electronic Structure

The electronic structure of a material not only helps in understanding the electron transfer mechanism in given material but also in several electronic properties. The general electronic structure and physical properties of perovskite related structures are governed by the following key energy terms, namely; i) On-site ( $U$ ) and inter-site ( $V$ ) Coulomb interactions, ii) Hund's coupling energy ( $JH$ ) which defines the transfer integral ( $t_{ij}$ ) and modifies the electron bandwidth ( $W$ ), iii) Charge transfer energy ( $\Delta$ ) arising due to crystal field splitting of transition metal  $3d$ -orbital in the presence of oxygen ligand  $2p$ - orbitals and iv) Electron-Phonon interaction (EPI) arising due to orbital ordering and/or Jahn-Teller (JT) distortion [39, 40]. The most important manganese (Mn) ion in the manganites having incomplete  $d$ -shell (Mn:  $[\text{Ar}] 3d^5 4s^2$ ) is surrounded by the oxygen octahedron which are the key players in determining the electronic properties of the manganites. For an isolated Mn atom, the  $3d$  levels present a five-fold degeneracy; however, in a manganite crystal an octahedron is formed by the six oxygen ions around the Mn atom. The compound  $\text{LaMnO}_3$  has been identified to possess characteristics of both Mott and charge transfer insulators. The estimated Mott–Hubbard interaction energy  $U_{dd}$  and charge transfer energy  $U_{pd}$ , lies between 4-6 eV [41-43]. The Mott-Hubbard interaction  $U_{dd}$  energy is required to create  $d^{n+1}d^{n-1}$  excitation in an array of  $d^n$  ions while the charge-transfer energy,  $U_{pd}$  is energy for creating  $p^5d^{n+1}$  charge excitation from  $p^6d^n$ , where  $n$  is the quantum

---

## [Chapter 1: Introduction]

---

state. In 3d transition metal group, the early oxides are Mott-Hubbard insulators whereas the last members are the charge-transfer insulators [44]. The Mn which exists in 3+ oxidation state in pure LaMnO<sub>3</sub> is converted to Mn<sup>4+</sup> due to doping of divalent cation. In the case of 3d ion, four electrons of Mn<sup>3+</sup> are in spin-up states with all unoccupied spin-down states. The five *d-orbitals* split in to ion/atom 3t<sub>2g</sub> and 2e<sub>g</sub> states by the crystal field of oxygen which are separated by the energy ~1.5 eV, 2.4 eV for Mn<sup>3+</sup> and Mn<sup>4+</sup> respectively [45]. For the intermediate doped manganites R<sub>1-x</sub>A<sub>x</sub>MnO<sub>3</sub> (0<x<1), Mn ions are in mixed valence states of Mn<sup>3+</sup> and Mn<sup>4+</sup>. A ratio of Mn<sup>3+</sup>/ Mn<sup>4+</sup> depends on the doping level ‘x’ of divalent element as (1-x)/x. In cubic lattice environment, the five-fold degenerate 3d - orbital splits into “t<sub>2g</sub>” and “e<sub>g</sub>” states [46]. The t<sub>2g</sub> level is in three lower energy levels while e<sub>g</sub> level has two higher energy levels with great potential for spintronics due to fully spin polarized condition. The strength of Hund’s coupling can modify the electronic structure which can result in to a higher t<sub>2g</sub><sup>↓</sup>/e<sub>g</sub><sup>2↑</sup> band with strong / weak Hund’s coupling [47]. Total spin and magnetic moment of Mn<sup>3+</sup> and Mn<sup>4+</sup> is 2 and 4 μB (μB =Bohr Magneton) and 3/2 and 3 μB, respectively.

### 1.3.3 Jahn-Teller Effect

The crystal field splitting arising from electronic structure and departure of the tolerance factor from unity discussed above are not the only cause of the structural distortion from ideal cubic structure in manganites. The Jahn-Teller effect due to strong electron–phonon interaction plays an important role in the systems after the inability of the double exchange (DE) to explain CMR properties [48].

According to Kramer’s degeneracy theorem the energy levels of a system having an odd number of spins show at least a residual degeneracy in the presence of pure/uniform electric field and can be lifted only by the application of magnetic field. Deformation of the oxygen

## [Chapter 1: Introduction]

octahedron causes energy degeneracy within the degenerate  $t_{2g}$  and  $e_g$  electron states. When the  $e_g$  shell is half filled it is energetically favorable to create a deformation because one of the orbitals will lose energy. The electrons in the  $e_g$  shell will then occupy this lower energy state. Creating a deformation of the oxygen octahedrons without altering the overall crystal lattice which leads to the typical JT distortions is shown in Fig. 1.4 [49, 50]. The JT distortion is responsible for lifting the degeneracy of  $3d$  -orbital in higher  $e_g$  ( $d_{x^2-y^2}$  and  $d_{3z^2-r^2}$ ) level and lower  $t_{2g}$  ( $d_{xy}$ ,  $d_{yz}$  and  $d_{zx}$ ) level in  $Mn^{3+}$  ion. The distortion of  $MnO_6$  octahedron is co-operative in nature and affects neighboring ions. The strong JT effect in the presence of  $e_g$  electron lowers the electronic energy and helps in binding the electron to a Mn ion. The distortion of the octahedron is maximum for  $x=0$ , but appears visible almost upto  $x=0.20$  [51].

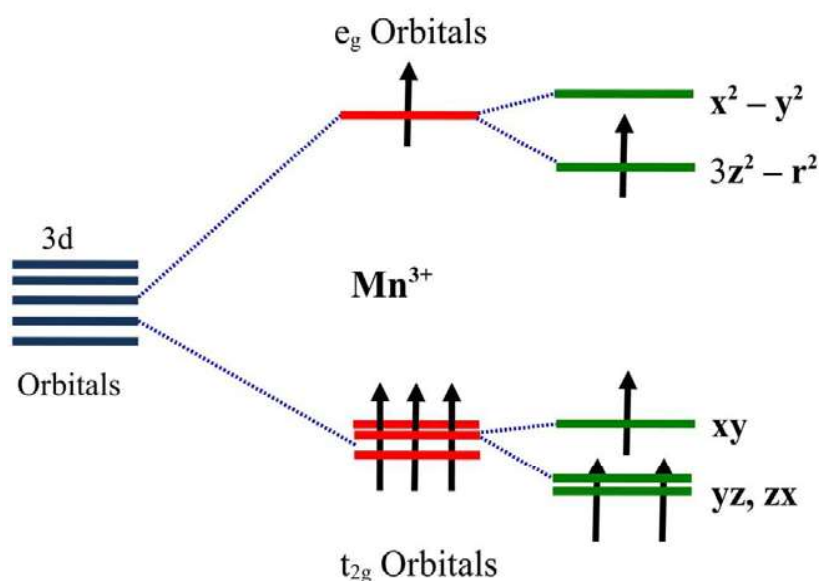


**Fig. 1.4:** Energy levels and orbitals of  $Mn^{4+}$  and  $Mn^{3+}$  in a crystal field in octahedral symmetry and with axial elongation [49,50].

### 1.3.4 Zener Double Exchange and Superexchange mechanism

In mixed-valent manganites, the conduction process between two Mn ions or simultaneously electrical resistance and magnetic ordering were explained by C. Zener in 1951

## [Chapter 1: Introduction]

[9, 10] and therefore is called “Zener-Double Exchange (ZDE)”. The knowledge of the electronic structure gives the necessary insight for understanding the ZDE conduction in the manganites. It has been reported that the lattice distortion brings down  $T_C$  by use of hole doping at Ln-site (A-site) suggesting tuning of  $T_C$  by hole doping and size of divalent cation. The simple manganites, such as  $\text{La}_{1-x}\text{M}_x\text{MnO}_3$  (M= Ca, Sr, Ba) with  $x = 0.33$  having strong DE exhibits a transition from high temperature paramagnetic (PM) semi- conducting or insulating (I) phase to a low temperature ferromagnetic phase.

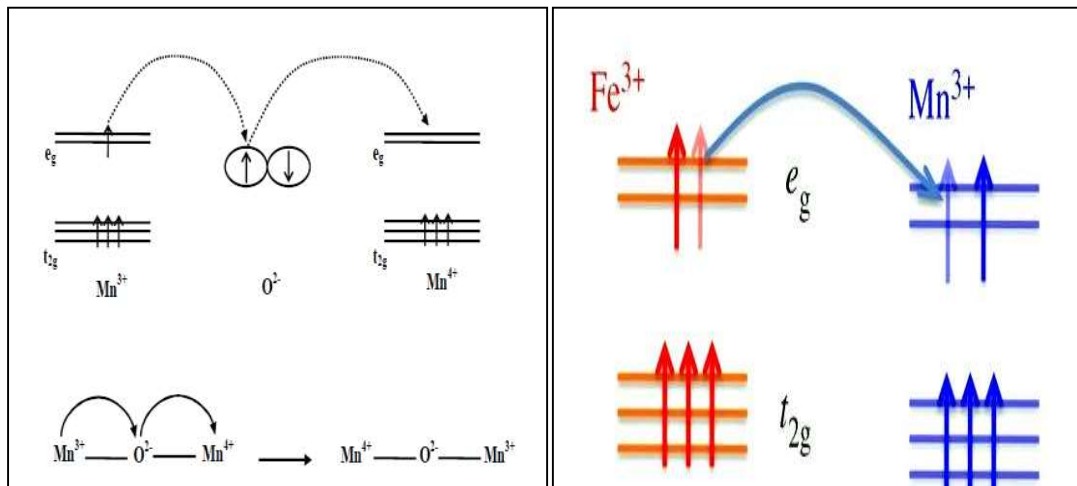


**Fig. 1.5:** Schematic representation of Zener-Double diagram.

The  $e_g$  electron of  $\text{Mn}^{3+}$  transfers to intermediate ligand oxygen which in turn transfers its electron to  $e_g$  level of  $\text{Mn}^{4+}$  ion. The double exchange origin from the electronic structure of the Mn site subjected to the crystal field created by the cubic symmetry surrounding the Mn site. The  $\text{Mn}^{3+}$  has an  $e_g$  electron on  $d_z^2$  orbital whereas  $\text{Mn}^{4+}$  has vacant  $e_g$  electron (Fig. 1.4). The  $e_g$  electron of  $\text{Mn}^{3+}$  experiences a net potential difference with respect to the vacant site of  $\text{Mn}^{4+}$  ion creating a tendency to hop to the vacant site. This is possible through the ligand oxygen having two 2p ( $\uparrow\downarrow$ ) electrons in the outermost orbital [52]. According to Hund’s rule the  $e_g$  electron of  $\text{Mn}^{3+}$  ion hops to spin up ( $\uparrow$ ) orbital of oxygen ion. The basic mechanism in this process is the

## [Chapter 1: Introduction]

doping of a d-hole from  $Mn^{4+}$  or electron doping from d-shell of  $Mn^{3+}$  to  $Mn^{4+}$  like  $Mn^{3+}$  via the oxygen, so that the  $Mn^{3+}$  and  $Mn^{4+}$  ions replace each other [10, 19]. The itinerant  $e_g$  electron retains its spin up state subjected to Hund's rule coupling. The ZDE is also spin polarized conduction and occurs only when the spins of the adjacent Mn ions are aligned in parallel direction or are ferromagnetically ordered. The deviation from this magnetic ordering between the spins of adjacent Mn ions decreases the ZDE and finally it vanishes after critical spin disorder. The other interaction known as superexchange is essential to understand the anti-ferromagnetic phase in highly doped manganites in absence of DE arising due to intermediate oxygen ion between Mn ions.

### 1.3.5 Phase diagram of $LaSrMnO_3$

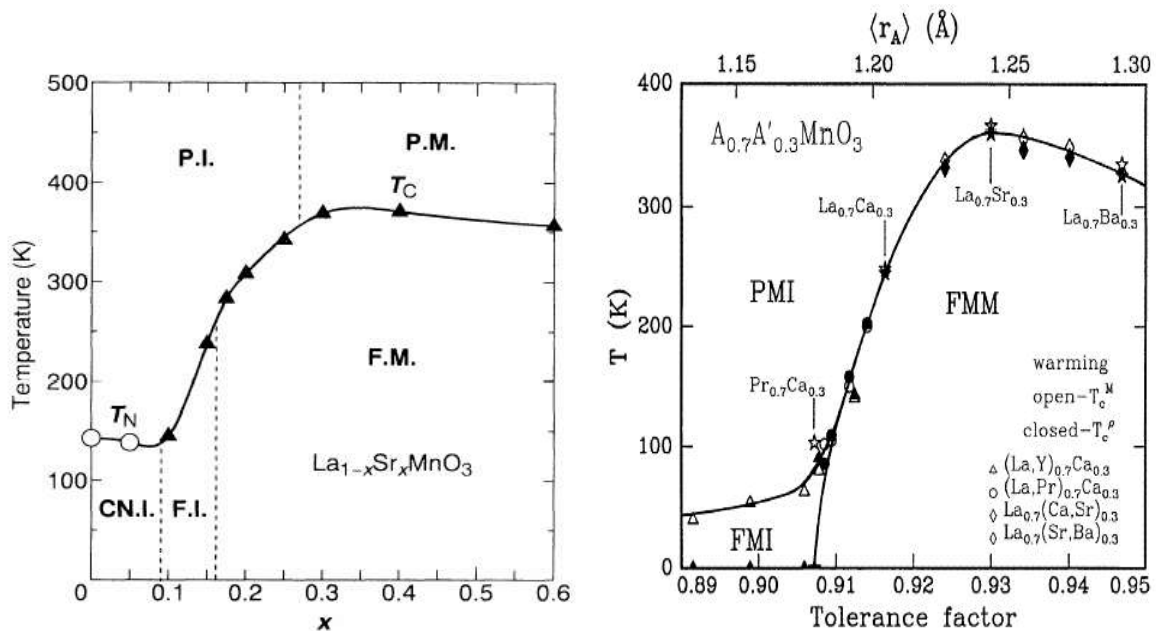


**Fig. 1.6:** Phase diagrams: (a) temperature versus concentration “x” and (b) temperature versus tolerance factor for  $A_{0.7}A'_{0.3}MnO_3$  [53].

The electronic phase diagram of large bandwidth system,  $La_{1-x}Sr_xMnO_3$  (LSMO) is shown in Fig. 1.6 [53]. It is found that the Ca-doped phase diagram is simple due to the absence of orthorhombic-rhombohedral structural phase transition contrast to the case of Sr-doped

## [Chapter 1: Introduction]

---

manganites due to many phases [54, 55]. There exist two distinct phases at high temperatures, paramagnetic insulator (PI) and paramagnetic metal (PM) (Fig. 1.6 (a)). In this figure PMI, FMI, FI, FM, PI and CI denote paramagnetic metal insulator, ferromagnetic metal insulator, ferromagnetic insulator, ferromagnetic metal, paramagnetic insulator, and spin canted insulator states, respectively [19, 53, 56, 57]. However, the crossover from metallic to insulating behavior occurs in a very narrow concentration region. A structural transition is observed at the lower concentration under field. The phase diagrams clearly show the concentration and tolerance factor dependent electronic and magnetic properties.

### 1.3.6 Size Variance at A and B-sites

The ionic mismatch due to the doping of divalent, alkaline earth cations or trivalent rare earth cations at A-site and transition metal ion at B-site results in the variety of interesting properties in manganites [52]. A linear relationship is found between  $T_C$  and  $\langle r_A \rangle$ . However, both of them exhibit inverse correlation with MR or CMR. The variation of  $\langle r_A \rangle$  at A-site cation in  $ABO_3$  perovskites has a similar effect like external pressure which enhances the B-O-B transfer integral through a change in B-O-B bond angle due to the distortion of  $BO_6$  octahedra for  $t < 1$  and narrowing the  $e_g$  electron bandwidth affecting electronic transport properties.

The substitution on B-site affects the  $Mn^{3+}-Mn^{4+}$  ratio and hence, there occurs an exchange interaction between  $Mn^{3+}-Mn^{4+}$ . The mismatch of ionic radius between Mn and substituted ions also has an impact on the lattice parameters. The minor change in Mn-O bond length and Mn-O-Mn bond angle in  $Mn^{3+}-O-Mn^{4+}$  network results in dramatic variation of the magnetic and transport properties of these manganites. B-site doping however in manganites directly affects the magnetic behavior and weakens the ferromagnetic interactions due to the decrease of manganese ions and reduction in DE. Hence, the Mn-site doping is an effective way

---

## [Chapter 1: Introduction]

---

to modify the crucial Mn-O-Mn network and in turn remarkably affects their intrinsic physical properties.

### 1.4 Applications of Colossal Magnetoresistance Materials

Basic research in the condensed matter physics and material science can lead to important developments in applied physics and engineering. The CMR spin-polarized conduction of carriers and M-I transition in manganites possess potential for various device applications mainly based on their transport properties [58, 59].

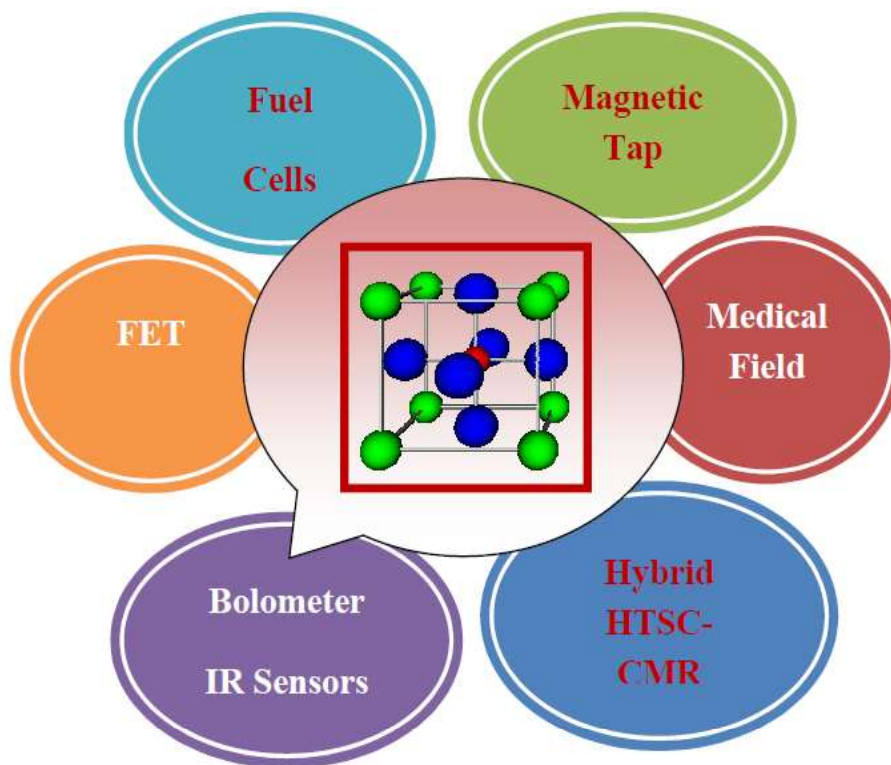


**Fig. 1.7:** Application of the Colossal Magnetoresistance manganite materials.

#### A. Magnetic Recording

Using CMR effect, the manganites have been utilized for magnetoresistive read-heads and magnetic memory devices. The write head is driven by a current source that carries the information to be stored in heads. The state of magnetization of the magnetic medium changes

---

## [Chapter 1: Introduction]

---

immediately due to change in magnetic flux and results into corresponding change in the resistivity.

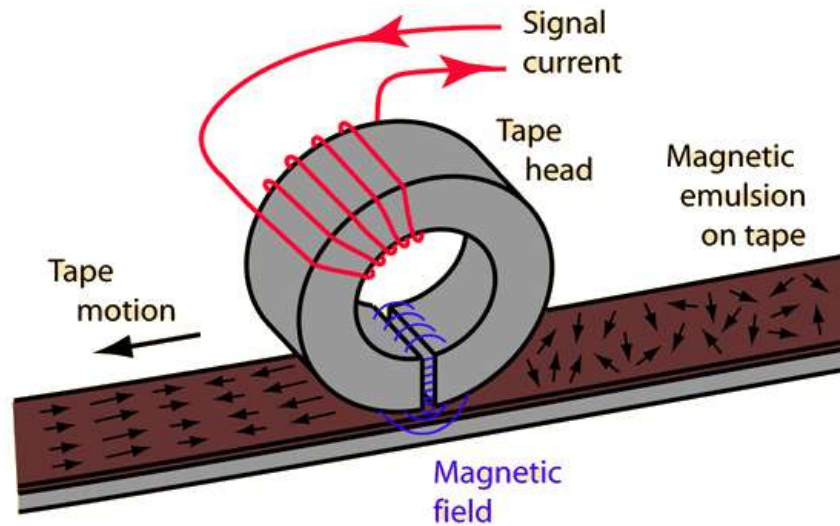


**Fig. 1.8:** Schematic diagram of the Tap recording [60].

The magnetization in the system is stored as “0” and “1” states in same and opposite directions respectively. The manganites could be utilized to make good memory read heads candidate if the MR% at the room temperature remains almost constant and about 20% in applied field of few hundred Oersted (Oe). The faster move of ferromagnetic material changes magnetic field more and results into the speed dependent induced current. Thus, the sensitivity of inductive read heads is limited by the precision of the material speed. The other limiting factor on inductive heads is the strength of the magnetic field. Hence, a continuous increase in storage density shrinks the size of a data element. Since fewer electrons are now contained in the region of one bit the associated magnetic field is smaller. This smaller magnetic field produces less change and thus less induced current, requiring more loops to produce a measurable current. Because of these limitations, new magnetic storage devices use the phenomenon of magnetoresistance to read magnetic data. The first step towards using the spin degree of

---

## [Chapter 1: Introduction]

---

freedom as a spin valve is magnetic multilayer composed of alternative ferromagnetic and nonmagnetic layers. The resistance of such a combined layer becomes lowest or highest when magnetic moment of both ferromagnetic layers is parallel or antiparallel respectively. This causes large magnetoresistance called GMR. Today, all computers and laptops use spin-valves in read heads of the hard disc. The density of stored data has reached the saturation with conventional spin-valves [61, 62].

### **B. IR sensors**

The bolometer is a resistive element constructed from a material with the large temperature coefficient of resistance to produce a large change in resistance to be used for measuring the radiated energy in the infrared and optical wavelength regions of the electromagnetic spectrum [63, 64]. The temperature coefficient of resistance (TCR) defined as  $1/R (dR/dT)$  evaluates the potentiality of any materials for bolometer sensors. While in  $\text{La}_{0.7}\text{Ca}_{0.3}\text{MnO}_3$ , TCR has been obtained as high as 10-18% in bulk form and the  $\text{La}_{0.7}\text{Sr}_{0.3}\text{MnO}_3$  manganite showed TCR of  $0.02 \text{ K}^{-1}$ , attracts interests due to its high Curie temperature ( $\sim 360 \text{ K}$ ), with the lower noise level compared to other manganites which makes it suitable candidate for bolometer fabrication [65]. The key factor is to find a high performance temperature sensing material, in terms of response and signal to noise ratio, thermally isolated structure in the smallest possible area. At the same time, it must be possible to integrate this material together with signal readout electronics. This bolometer operates on a conductivity transition in which the electrical resistance changes dramatically over the transition temperature range.

### **C. Hybrid HTSC-CMR devices**

Another important use of the CMR materials is in high temperature superconductor–colossal magnetoresistance (HTSC-CMR) hybrid devices. The HTSC-CMR spin injection device uses

## [Chapter 1: Introduction]

---

spin polarized electrons from the manganite layers and are injected into the HTSC channel layers. In this device the gate current dependent I-V characteristics are studied. In these devices, current flows in the CMR layer responsible for the decreases of critical current density ( $J_C$ ) of superconducting layer due to pair breaking phenomenon of spin-polarized carriers [66-68]. This property largely differs when CMR layer with spin polarization character is replaced with the one having un-polarized electrons as carriers. Spin polarized carrier increases the pair breaking efficiency by many folds.

### **D. Electric Field Effect Devices**

Manganites have also been used in field effect transistors (FET). The FET is realized on the concept of a methodology where electric field controls the shape and conductivity of channel. FETs based on CMR channel show interesting characteristics depending on the dielectric layer [69]. This device is used in understanding the fall of polarization with increasing Curie temperature. The ferroelectric gate devices show large changes in resistance (as large as  $\sim 100\%$ ), which make them attractive for potential non-volatile applications [52].

### **E. Biomedical Applications**

The CMR materials have great deal of interests in the biomedical applications like bio-detectors and magneto-controlled drug delivery systems. However, the most attractive area of application for these manganites in recent times is self controlled magnetic hyperthermia of internal tumors and targeted drug delivery. Magnetic hyperthermia is a prospective method for cancer treatment based on higher sensitivity of tumor cell to thermal treatment at 30-40°C. A substantial disadvantage of the current availability in  $Fe_3O_4$  based magnetic mediators is the lack of point-to-point temperature control during treatment of internal tumors. This problem could be solved by the development of smart magnetic mediator based on manganites with appropriate

## [Chapter 1: Introduction]

---

low Curie temperature. The magnetic particles lose ferromagnetic ordering when they approach  $T_C$  and stop producing heat caused by magnetization reversal in alternating magnetic field [70].

### 1.5 Motivation of the present work

The present work is a blend of investigations of various physical properties aimed both at the understanding of the physics involved and the analysis of an important class of compounds called as manganites revived great deal of attention from application point of view. During the present work, we have synthesized the trivalent earth element  $Fe^{3+}$  doped manganites using the two important methods namely the planetary ball milling and sol-gel routes for wide range of temperature and doping concentration. The present work is mainly aimed towards understanding and detecting the best synthesis route for fabricating the nano scale polycrystalline manganite systems out of the selected two methods; the ball milling and sol-gel routes in terms of time duration, low reaction time, annealing temperature and cost-effectiveness with the help of *state-of-the-art* density functional theory (DFT) based first principles calculations. The manganite system investigated during the present work is  $La_{0.67}Sr_{0.33}Mn_{1-x}Fe_xO_3$  ( $x=0.15, 0.25$  and  $0.35$ ). The Fe doped  $La_{0.67}Sr_{0.33}MnO_3$  (LSMO) manganite systems have revealed several interesting results on the structural, electronic, magnetic and vibrational properties. Looking to the importance of structure–property relation a systematic study and analysis of the bond length and bond angle dependent structural, magnetic and vibrational properties using XRD is performed. In addition, the effect of grain size and grain morphology on various properties of nanostructured  $La_{0.67}Sr_{0.33}Mn_{1-x}Fe_xO_3$  ( $x=0.15, 0.25$  and  $0.35$ ) manganites synthesized using both routes have been carried out. Furthermore, interesting part of the thesis work is to understand the manganite properties with the clear insight into the responsible mechanism achieved by performing the atomistic high-throughput calculations under the framework of the *state-of-the-art* density

## [Chapter 1: Introduction]

---

functional theory. The good agreement between the experimentally synthesized and characterized manganite systems with the first-principles based DFT results once again prove the reliability of DFT based *ab initio* calculations and also significantly contributes to the theoretical database by adding up the missing details on the considered manganites. The DFT calculations clearly bring out the possibility of formation of the manganite through formation energy calculation. The calculated structural, electronic and vibrational properties help in understanding the reason of preferred methods of synthesis for manganites. The specific motivation of the present work is as follows:

1. Synthesis of manganite samples using two synthesis routes: Ball milling and Sol-gel.
2. Effect of doping of Fe at Mn site on properties of manganites.
3. Using DFT studies identify the best route out of two above mentioned synthesis routes of manganites. For this structure property relation together with the formation energy analysis analyzed using their own experimental parameter.

### 1.6 Plan of the Thesis

The aim of the present thesis was to study the effect of Fe doping at Mn site on the properties of CMR material  $\text{La}_{0.67}\text{Sr}_{0.33}\text{MnO}_3$  synthesized using two different routes and analyze them with the help of suitable characterization techniques and *state-of-the-art* density functional theory based first principles calculations.

### Chapter [2]

**Chapter 2** deals with the various experimental tools and methods to discuss the synthesis and characterization techniques to determine the properties of the Fe doped LSMO such as structural, elemental, magnetic, vibrational etc. This chapter also discusses the details about the methodology for preparing the polycrystalline doped manganite compounds using sol-gel and

## [Chapter 1: Introduction]

---

ball milling methods. Various characterization methods to understand the structural relation with the properties of LSMO manganites have been discussed. The working and operation of the X-ray diffraction for structural analysis, PPMS Quantum Design magnetometer to study the magnetic properties, Field emission electron microscope (FE-SEM) to study the surface morphology and Raman spectroscopy for vibrational properties are also presented.

### Chapter [3]

**Chapter 3** presents the brief description of the density functional theory starting with the history and need for its development. Original construction of Hohenberg and Kohn is discussed. The chapter also introduces a methodology to treat the calculation of ground state properties of the system based on Kohn-Sham formulation of DFT, which is based on the approximations for the exchange energy term. A brief layout of Vienna Ab-initio Simulation Package (VASP) utilized for computing the proposed properties of the systems is also presented.

### Chapter [4]

**Chapter 4** deals with the real research problem and efforts to resolve some issues in the related field. The structural, surface morphological, vibrational and magnetic properties of  $\text{La}_{0.67}\text{Sr}_{0.33}\text{Mn}_{1-x}\text{Fe}_x\text{O}_3$  ( $x=0.15, 0.25$  and  $0.35$ ) synthesized using ball milling method are presented. The comparison of the results with the available outcome of the material is analyzed on the basis of different concentrations and temperature employed on the samples. The density functional theory calculations for the formation energy, electronic and vibrational properties are discussed and correlated with the experimental results.

### Chapter [5]

In this chapter, the structural, surface morphological, vibrational and magnetic properties of  $\text{La}_{0.67}\text{Sr}_{0.33}\text{Mn}_{1-x}\text{Fe}_x\text{O}_3$  ( $x=0.15, 0.25$  and  $0.35$ ) synthesized using sol-gel method is discussed.

## [Chapter 1: Introduction]

---

The comparison of results with different composition as well as temperature employed to the samples is thoroughly discussed. Thus, here we present the results of experimental study to understand the relationship of small amount of Fe doping with the various properties. We make the attempt to compare the results of samples obtained from planetary ball milling and sol-gel route together with the DFT calculations to find the simple, easiest way to synthesize the polycrystalline CMR materials.

### Chapter [6]

This chapter presents the conclusion based on the comparative study of manganite samples  $\text{La}_{0.67}\text{Sr}_{0.33}\text{Mn}_{1-x}\text{Fe}_x\text{O}_3$  (LSMFO) prepared using two experimental techniques ball milling and sol-gel for different concentrations of iron and calcination temperatures. We have used density functional theory based high-throughput calculations to draw a significant conclusion to understand the formation of LSMFO prepared using two different methods. We have considered same concentration of iron doping and calcination temperatures for understanding the technique dependent synthesis and relevant properties. The structure property relation obtained through different characterization techniques has been analyzed and understood at atomic level. The electronic band structures and phonon modes obtained using density functional theory have been used to interpret the valence band spectra, magnetization and Raman spectra obtained from various corresponding experimental techniques. An analysis in the conclusion chapter is put forward to justify the differences in the properties of manganite samples prepared using mentioned techniques.

## [Chapter 1: Introduction]

---

### References

1. G. H. Jonker and V. Sathe, *Physica* 16, 337 (1950).
2. A. Congeduti, P. Postorino, P. Dore, A. Nucara, S. Lupi, S. Mercone, P. Calvani, A. Kumar and D. D. Sarma, *Physical Review B* 63, 184410 (2001).
3. C. N. R. Rao and B. Raveau (2 ed) "Transition Metal Oxides: Structure, Properties and Synthesis of Ceramic Oxides" John Willey and Sons, Inc. pp. 392 (1998).
4. H. Reshi and V. Shelke, *J. Nano-Electronic Phys.* 5, 04053 (2013).
5. E. L. Nagaev, *Physics Reports* 346, 387 (2001).
6. A. J. Millis, *Nature Macmillan Publishers Ltd* 392, 147 (1998).
7. A. M. Haghiri-Gosnet and J. P. Renard, *J. Phys. D: Appl. Phys.* 36, R127 (2003).
8. P. K. Jha, *Physical Review B* 72, 214502 (2005).
9. C. Zener, *Phys. Rev.* 81, 440 (1951).
10. C. Zener, *Phys. Rev.* 82, 403 (1951).
11. E. Pollert, S. Krupicka and E. Kuzwiczova, *J. Phys. Chem. Solids* 43, 1137 (1982).
12. G. Zhao, K. Conder, H. Keller and K.A. Muller, *Nature* 381, 676 (1996).
13. S. A. Wolf, D. D. Awschalom, R. A. Buhrman, J. M. Daughton, S. von Molnar, M. L. Roukes, A. Y. Chtchelkanova and D. M. Treger, *Science* 294, 1488 (2001).
14. M. Tondra, J. M. Daughton, D. Wang, R. S. Beech, A. Fink and J. A. Taylor, *J. Appl. Phys.* 83, 6688 (1998).
15. G. A. Prinz, *Science* 282, 1660 (1998).
16. K. Kobayashi, T. Kimura, H. Sawada, K. Terakura and Y. Tokura, *Nature* 395, 677 (1998).
17. C. N. R. Rao and B. Raveau "Colossal Magnetoresistance, charge ordering and other related properties of rare earth manganates", World Scientific Publishing Company, pp. 356 (1998).
18. Y. Tokura, "Magnetoresistive oxides" Gordon and Breach publishes, London 2, pp. 358 (2000).
19. J. M. D. Coey, M. Viret and S. Von Molnar, "Mixed valent manganites" *Advances in Phys.* 48, 167 (1999).
20. A.P. Ramirez, *J. Phys: Condens. Matter* 9, 8171 (1999).
21. A. M. H. Gosnet and J. P. Renard, *J. Phys. D: Appl. Phys.* 36, R127 (2003).

## [Chapter 1: Introduction]

---

22. P. Schiffer, A. P. Ramirez, W. Bao and S.W. Cheong, *Phys. Rev. Lett.* 75, 3336 (1995).
23. S. Jin, T. H. Tiefel, M. McCormack, R. A. Fastnacht, R. Ramesh and L. H. Chen, *Science* 264, 413 (1994).
24. G. H. Jonker and J. H. Van Santen, *Physica (Utrecht)* 16, 337 (1950).
25. W. Thomson, "On the Electro-Dynamic Qualities of Metals:—Effects of Magnetization on the Electric Conductivity of Nickel and of Iron", *Proc. Royal Soc. Lond.* 8, pp. 546 (1857).
26. T. McGuire and R. Potter, *IEEE Transactions on Magnetism* 11, 1018 (1975).
27. A. Malozemoff, *Physical Review B* 32, 6080 (1985).
28. M. Julliere, *Phys. Lett.* 54A, 225 (1975).
29. H.Y. Hwang, S.W. Cheong, N.P. Ong and B. Batlogg, *Phys. Rev. Lett.* 77, 2041 (1996).
30. J. S. Hellman and B. Abeles, *Phys. Rev. Lett.* 37, 1429 (1976).
31. [https://en.wikipedia.org/wiki/Tunnel\\_magnetoresistance](https://en.wikipedia.org/wiki/Tunnel_magnetoresistance).
32. C. Reig, M. Dolores Cubells Beltran and D. Ramirez Munoz, *Sensors* 9, 7919 (2009).
33. E. Hirota, H. Sakakima and K. Inomata, *Giant Magneto-Resistance Devices*, Springer 40, pp. 177 (2002).
34. D. S. Rana, C. M. Thaker, K. R. Mavani, D. G. Kuberkar, Darshan C. Kundaliya and S. K. Malik, *J. Appl. Phys.* 95, 4934 (2004).
35. R. Mahesh, R. Mahendiran, A. K. Raychaudhuri and C.N.R. Rao, *J. Solid State Chem.* 114, 297 (1995).
36. R. Von Helmolt, J. Wecker, B. Holzapfel, L. Schultz and K. Samwer, *Phys. Rev. Lett.* 71, 331 (1993).
37. K. Chahara, T. Ohno, M. Kasai and Y. Kosono, *Appl. Phys. Lett.* 63, 1990 (1993).
38. E. Dagotto, T. Hotta and A. Moreo, *Physics Report* 344, 1 (2001).
39. E. Dagotto, "Nanoscale Phase Separation and Colossal Magnetoresistance the Physics of Manganites and Related Compounds", Springer Verlag Berlin and Heidelberg GmbH, 136, pp. 459 (2002).
40. Y. Tokura, *Rep. Prog. Phys.* 69, 797 (2006).
41. J. Zaanen, G.A. Sawatzky and J.W. Allen, *Phys. Rev. Lett.* 55, 418 (1985).
42. J. Zaanen and G.A. Sawatzky, *J. Solid state Chem.* 88, 8 (1990).

## [Chapter 1: Introduction]

---

43. J. H. Park, C.T. Chen, S. W. Cheong, W. Bao, G. Meigs, V. Chakarian and Y.U. Idzerda, *Phys. Rev. Lett.* 76, 4215 (1996).
44. A. K. Raychaudhuri, *Advances in Physics* 44, 21 (1995).
45. M. Abbate, F.M.F. De Groot, J.C. Fuggle, A. Fujimori, O. Strebel, F. Lopez, M. Domke, G. Kaindl, G.A. Sawatzky, M. Takano, Y. Takeda, H. Eisaki and S. Uchida, *Phys. Rev. B* 46, 4511 (1992).
46. J. Goodenough, *Magnetism and Chemical Bond*, Interscience Publisher, New York, London, pp. 385 (1963).
47. L. Yu Kuai, Y. Yue Wei and L. X. Guang, *Chin. Phys. B* 22, 087502 (2013).
48. A. J. Millis, P. B. Littlewood and B. I. Shraiman, *Phys. Rev. Lett.* 74, 5144 (1995).
49. H. A. Jahn and E. Teller, *Proc. R. Soc. London A* 161, 220 (1937).
50. Y. Tokura, *Reports on Progress in Physics* 69, 797 (2006).
51. K. Pradhan, “The Impact of B Site Disorder in the Manganites”, PhD thesis, Harish Chandra Research Institute, Allahabad (2009).
52. Y. Okimoto, T. Katsufuji, T. Ishikawa, A. Urushibara, T. Arima and Y. Tokura, *Phys. Rev. Lett.* 75, 109 (1995).
53. H. Y. Hwang, S. W. Cheong, P. G. Radaelli, M. Marezio and B. Batlogg, *Phys. Rev. Lett.* 75, 914 (1995).
54. M. Talati and P. K. Jha, “Vibrational properties of some colossal magnetoresistance materials”, PhD thesis, Maharaja Sayajirao University of Baroda, Vadodara (2006).
55. Y. Yamada, O. Hino, S. Nohdo, R. Kanao, T. Inami and S. Katano, *Phys. Rev. Lett.* 77, 904 (1996).
56. Y. Tokura, Y. Tomioka, H. Kuwahara, A. Asamitsu, Y. Morimoto and M. Kasai, *J. Appl. Phys.* 79, 5288 (1998).
57. A. Urushibara, Y. Moritomo, T. Arima, A. Asamitsu, G. Kido and Y. Tokura, *Phys. Rev. B* 51, 14103 (1995).
58. T. Venkatesan, M. Rajeswari, Z. W. Dong, S.B. Ogale and R. Ramesh, *Phil. Trans. R. Soc. Lond. A* 356, 1693 (1998).
59. N. D. Mathur, G. Burnell, S. P. Isaac, T. J. Jackson, B. S. Teo, J. L. MacManus Dricoll, L. F. Cohen, I. E. Evetts and M. G. Blamire, *Nature* 387, 266 (1997).
60. <http://hyperphysics.phy-astr.gsu.edu/hbase/Audio/tape2.html>.

## [Chapter 1: Introduction]

---

61. S. P. Vachhani, "Investigations on mixed valent manganites", PhD thesis, Saurashtra University, Rajkot (2008).
62. G. Binasch, P. Grunberg, F. Saurenbach and W. Zinn, *Phys. Rev. B* 39, 4828 (1989).
63. A. Goyal, M. Reijeswari, R. Shrakala, S. E. Lofland, S. M. Bhagat, T. Boettcher, C. Kwon, R. Ramesh and T. Venkatesan, *Appl. Phys. Lett.* 71, 2535 (1997).
64. M. Rajeswari, C. H. Chen, A. Goyal, C. Kwo, M. C. Robson, R. Ramesh, T. Venkatesan, and S. Lakeou, *Appl. Phys. Lett.* 68, 3555 (1996)
65. S. P. Langley, "The bolometer", *Proceedings of The American Metrological Society* 2, 184 (1880).
66. A. Lisauskas, S. Khartsev and A. Grishin, *Appl. Phys. Lett.* 77, 3302 (2000).
67. Z. W. Dong, R. Ramesh, T. Venkatesan, M. Johnson, Z.Y. Chen, S.P. Pai, V. Talyansky, R.P. Sharma, R. Shreekala, C. J. Lobb and R. L. Greene, *Appl. Phys. Lett.* 71, 1718 (1997).
68. T. Kimura, Y. Tomioka, H. Kuwahara, A. Asamitsu, M. Tamura and Y. Tokura, *Science* 274, 1698 (1996).
69. S.B. Ogale, V. Talyansky, C.H. Chen, R. Ramesh, R. L. Greene, T. Venktesan, *Phys. Rev. Lett.* 77, 1159 (1996).
70. O. Shlyakhtin, V. Leontiev, O. Young Jei and A. Kuznetsov, *Smart Materials and Structures*, 16, N35 (2007).